Available online at www.sciencedirect.com
SCIENCE DIRECT®
ELSEVIER
International Journal of Solids and Structures 43 (2006) 1047–1060
INTERNATIONAL JOURNAL OF SOLIDS and STRUCTURES
www.elsevier.com/locate/ijsolstr

A comparison of cohesive zone modeling and classical fracture mechanics based on near tip stress field

Z.-H. Jin [1], C.T. Sun *

School of Aeronautics and Astronautics, Purdue University, 325 N. Grant Street, West Lafayette, IN 47907, USA

Received 26 October 2004; received in revised form 17 June 2005
Available online 30 August 2005

Abstract

A mode III crack with a cohesive zone in a power-law hardening material is studied under small scale yielding conditions. The cohesive law follows a softening path with the peak traction at the start of separation process. The stress and strain fields in the plastic zone, and the cohesive traction and separation displacement in the cohesive zone are obtained. The results show that for a modest hardening material (with a hardening exponent $N = 0.3$), the stress distribution in a large portion of the plastic zone is significantly altered with the introduction of the cohesive zone if the peak cohesive traction is less than two times yield stress, which implies the disparity in terms of the fracture prediction between the classical approach of elastic–plastic fracture mechanics and the cohesive zone approach. The stress distributions with and without the cohesive zone converge when the peak cohesive traction becomes infinitely large. A qualitative study on the equivalency between the cohesive zone approach and the classical linear elastic fracture mechanics indicates that smaller cracks require a higher peak cohesive traction than that for longer cracks if similar fracture initiations are to be predicted by the two approaches.

Keywords: Cohesive zone; Cohesive traction; Fracture mechanics; Elastic–plastic deformation; Antiplane shear

1. Introduction

In recent years, the cohesive zone modeling approach has emerged as a popular tool for investigating fracture processes in materials and structures (see, for example, Needleman, 1987; Tvergaard and Hutchinson, 1992; Xu and Needleman, 1994; Ortiz and Pandolfi, 1999; Roy and Dodds, 2001; Elices et al., 2002;

* Corresponding author. Tel.: +1 765 494 5130; fax: +1 765 494 0307.
E-mail address: sun@ecn.purdue.edu (C.T. Sun).
[1] Present address: Department of Mechanical Engineering, The University of Maine, Orono, ME 04469, USA.

0020-7683/$ - see front matter © 2005 Elsevier Ltd. All rights reserved.
doi:10.1016/j.ijsolstr.2005.06.074

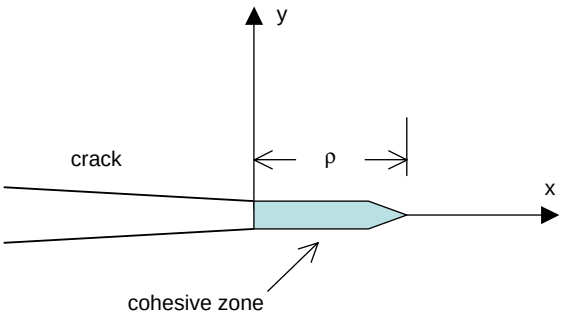

Fig. 1. A cohesive zone ahead of a crack.

de Borst, 2003; Scheider and Brocks, 2003; Jin and Sun, 2005a). In a cohesive zone model, a narrow-band of vanishing thickness termed the cohesive zone is assumed to exist ahead of a crack tip (see Fig. 1) to represent the fracture process zone. The upper and lower surfaces of the narrow-band are termed as the cohesive surfaces and are acted by the so-called cohesive traction which follows a cohesive constitutive law that relates the cohesive traction to the separation displacement of the cohesive surfaces. Crack growth occurs when the separation at the tail of the cohesive zone (physical crack tip) reaches a critical value at which the cohesive traction vanishes. Clearly, the cohesive zone modeling approach does not involve crack tip stress singularities in classical fracture mechanics, and material failure is controlled by quantities such as displacements and stresses, which are consistent with the usual strength of materials theory.

Barenblatt (1962) proposed a cohesive fracture concept aiming to eliminate the crack tip stress singularity in the classical linear elastic fracture mechanics (LEFM). The strip yield zone model of Dugdale (1960), which was proposed for estimating the crack tip plastic zone size, has also been regarded as a cohesive zone type model with the strip yield zone treated as a cohesive zone. Mathematically, a cohesive zone model is described by a cohesive law or the relationship between the cohesive traction σ and the opening displacement (separation) δ of the cohesive surfaces as follows:

$$\sigma = \sigma_c f(\delta/\delta_c), \tag{1}$$

where σ_c is the peak cohesive traction, δ_c a characteristic opening, and f a dimensionless function describing the 'shape' of the cohesive traction–separation curve (cohesive curve). A fundamental parameter of the cohesive zone model (1) is the cohesive energy density, or the work of separation per unit area of cohesive surface, defined by

$$\Gamma_c = \int_0^\infty \sigma(\delta)\,\mathrm{d}\delta. \tag{2}$$

Although the cohesive zone modeling approach has been used by many authors for more than a decade, the physical reality of the cohesive zone is still an issue for debate. Since it has no thickness but has a limiting stress level that affects the stress field in the region surrounding it, the cohesive zone model cannot be identical to the classical continuum fracture mechanics. In recent years, there have been attempts to interpret some of the distinct narrow deformation bands (e.g., necking in ductile thin sheets and crazing in some polymers) that are generated ahead of the crack tip as a cohesive zone. For these physical "cohesive zones", the cohesive characteristics (σ_c, δ_c, Γ_c and f in (1) and (2)) may be determined directly by analyzing the stress and deformation states in the band. For example, Jin and Sun (2005b) developed a cohesive zone model for ductile thin sheet materials by treating the crack front necking zone as the cohesive zone. If such a distinct narrow deformation band is not present, the cohesive zone can only be regarded a hypothesis or an approximate representation of the crack tip process zone and, consequently, the cohesive zone param-

eters can only be determined by matching the fracture test result. In this case, the stress field near a crack tip with a cohesive zone should be approximately the same as the singular field of classical fracture mechanics except in the cohesive zone and its immediate vicinity. These considerations may place some restrictions on the selection of cohesive zone parameters.

The purpose of the present work is to investigate the equivalency between the cohesive zone modeling and the classical fracture mechanics by considering the influence of the cohesive zone on the crack tip stress field in elastic–plastic materials. A mode III crack with a fully developed cohesive zone in an elastic power-law hardening material is studied under small scale yielding conditions. A particular cohesive law is assumed to follow a softening path with the peak traction at the start of separation process. The stress and strain fields in the plastic zone and the cohesive traction and separation displacement in the cohesive zone are obtained. Effects of the cohesive zone parameters on the stress distribution are discussed. The influence of the peak cohesive traction on the equivalency between the cohesive zone approach and LEFM is also investigated.

2. Cohesive zone modeling and EPFM

Elastic–plastic fracture mechanics (EPFM) has been less successful than LEFM in predicting fracture of materials and structures, especially when large scale yielding prevails. Under small scale yielding conditions, however, Irwin's corrected stress intensity factor K may be employed to predict the resistance curve. If the cohesive zone approach is to be considered equivalent to the classical approach of EPFM as a rigorous engineering tool capable of predicting material fracture, the stress fields from the two approaches should match in the region dominated by the singular field of EPFM except in the cohesive zone and its immediate vicinity. In this section, the small scale yielding solution is introduced for a mode III crack with a *fully developed* cohesive zone in an elastic power-law hardening material. The cohesive law is assumed to follow a softening path with the peak traction occurring at the start of separation. The effect of the cohesive zone parameters on the crack tip stress distribution is studied.

2.1. Basic equations

Under mode III (antiplane shear) deformation conditions, there are only five nonzero field quantities independent of the coordinate z, i.e.,

$$\begin{aligned} &\tau_x = \sigma_{xz}, \quad \tau_y = \sigma_{yz}, \\ &\gamma_x = 2\varepsilon_{xz}, \quad \gamma_y = 2\varepsilon_{yz}, \\ &w = u_z. \end{aligned} \tag{3}$$

These field variables satisfy the equilibrium equation

$$\frac{\partial \tau_x}{\partial x} + \frac{\partial \tau_y}{\partial y} = 0 \tag{4}$$

the strain–displacement relationship

$$\gamma_x = \frac{\partial w}{\partial x}, \quad \gamma_y = \frac{\partial w}{\partial y} \tag{5}$$

and the constitutive law

$$\tau_x = \left(\frac{\tau_e}{\gamma_e}\right)\gamma_x, \quad \tau_y = \left(\frac{\tau_e}{\gamma_e}\right)\gamma_y, \tag{6}$$

where

$$\tau_e = \sqrt{\tau_x^2 + \tau_y^2}, \quad \gamma_e = \sqrt{\gamma_x^2 + \gamma_y^2} \tag{7}$$

are the effective shear stress and shear strain, respectively. For an elastic power-law hardening material, τ_e and γ_e are related by

$$\begin{aligned} \tau_e &= \mu\gamma_e, \quad \gamma_e \le \gamma_0, \\ &= \tau_0(\gamma_e/\gamma_0)^N, \quad \gamma_e \ge \gamma_0 \end{aligned} \tag{8}$$

in which μ is the shear modulus, τ_0 is the yield stress in shear, $\gamma_0 = \tau_0/\mu$ is the yield strain in shear, and N is the hardening exponent. Here the deformation plasticity is used, which is appropriate for stationary crack problems.

Under small scale yielding conditions, we can consider a semi-infinite crack with a cohesive zone of length ρ, as shown in Fig. 1. The symmetry condition along the crack/cohesive zone extended line ($x > \rho, y = 0$) and the crack face traction-free condition ($x < 0, y = 0$) are

$$\begin{aligned} &\gamma_x = 0, \quad x > \rho, \quad y = 0, \\ &\tau_y = 0, \quad x < 0, \quad y = 0. \end{aligned} \tag{9}$$

Along the cohesive zone ($0 < x < \rho, y = 0$), we assume that the cohesive traction, τ, is described by the following specific distribution:

$$\tau = \tau_y = \tau_c \cos\chi, \quad 0 < x < \rho, \quad y = 0, \tag{10}$$

where τ_c is the peak cohesive traction and χ varies from 0 at $x = \rho$ (cohesive zone tip) to $\pi/2$ at $x = 0$ (physical crack tip) so that $\tau = \tau_c$ at $x = \rho$ and $\tau = 0$ at $x = 0$, i.e., the cohesive zone is fully developed. Although the assumed cohesive traction of (10) is for mathematical convenience, it is in accordance with physical interpretations of a softening law. It is noted that we take the approach by posing the problem with the cohesive law to be determined later (i.e., χ will be related to the separation displacement).

The boundary conditions (9) and (10) are supplemented by the following asymptotic conditions of small scale yielding:

$$\tau_y + i\tau_x \to \frac{K_{III}^2}{\sqrt{2\pi z}}, \quad |z|/R \to \infty, \tag{11}$$

where K_{III} is the applied mode III stress intensity factor, $z = x + iy$, and R scales with the plastic zone size.

The above mode III crack problem may be treated analytically by using the Hodograph method (see, for example, Rice, 1968). In the Hodograph method, the basic nonlinear equations in the physical plane are transformed into the following linear equations about the strain function, ψ, in the strain plane:

$$\frac{\partial^2\psi}{\partial\gamma_e^2} + \frac{1}{\gamma_e}\frac{\partial\psi}{\partial\gamma_e} + \frac{1}{\gamma_e^2}\frac{\partial^2\psi}{\partial\varphi^2} = 0 \tag{12}$$

in the elastic zone ($\gamma_e < \gamma_0$), and

$$\frac{\partial^2\psi}{\partial\gamma_e^2} + \frac{N}{\gamma_e}\frac{\partial\psi}{\partial\gamma_e} + \frac{N}{\gamma_e^2}\frac{\partial^2\psi}{\partial\varphi^2} = 0 \tag{13}$$

in the plastic zone ($\gamma_0 < \gamma_e < \gamma_c$), where φ is an angle defined by

$$\tau_x = -\tau_e \sin\varphi, \quad \tau_y = \tau_e \cos\varphi, \tag{14}$$

$$\gamma_x = -\gamma_e \sin\varphi, \quad \gamma_y = \gamma_e \cos\varphi \tag{15}$$

and γ_e and φ are related to the coordinates (x, y) through ψ by

$$x = -\sin\varphi\frac{\partial\psi}{\partial\gamma_e} - \frac{\cos\varphi}{\gamma_e}\frac{\partial\psi}{\partial\varphi}, \quad y = \cos\varphi\frac{\partial\psi}{\partial\gamma_e} - \frac{\sin\varphi}{\gamma_e}\frac{\partial\psi}{\partial\varphi}. \tag{16}$$

The boundary conditions for ψ in the strain plane are obtained by transforming (9)–(11). By setting χ in (10) as φ, and for a fully developed cohesive zone, we have

$$\begin{aligned} &\frac{\partial\psi}{\partial\gamma_e} = 0, \quad \varphi = 0, \\ &\frac{\partial\psi}{\partial\varphi} = 0, \quad \varphi = \frac{\pi}{2} \end{aligned} \tag{17}$$

and

$$\cos\varphi\frac{\partial\psi}{\partial\gamma_e} - \frac{\sin\varphi}{\gamma_e}\frac{\partial\psi}{\partial\varphi} = 0, \quad \gamma_e = \gamma_c, \tag{18}$$

where γ_c is

$$\gamma_c = \gamma_0\left(\frac{\tau_c}{\tau_0}\right)^{1/N}. \tag{19}$$

The small scale yielding asymptotic condition now becomes

$$\psi \to -\frac{K_{III}^2}{2\pi\mu^2}\frac{\sin\varphi}{\gamma_e}, \quad \gamma_e \to 0. \tag{20}$$

2.2. Solution of $\psi(\gamma_e, \varphi)$

The governing equations (12) and (13) may be solved using the separation of variables method (see details in Rice (1968)). After considering the boundary conditions (17)–(20) and the continuity conditions across the elastic–plastic boundary, the solution $\psi(\gamma_e, \varphi)$ can be obtained. In the elastic region $(0 < \gamma_e < \gamma_0)$, we have

$$\begin{aligned} \psi = &\left\{\left[\left(\frac{\gamma_0}{\gamma_c}\right)^{1+N} - 1\right]\frac{1-N}{1+N}\frac{\gamma_e}{\gamma_0} - \frac{\gamma_0}{\gamma_e}\right\}(\gamma_0 R)\sin\varphi \\ &+ \sum_{k=2}^{\infty}(\beta_k - \alpha_k)H_k\left(\frac{\gamma_e}{\gamma_0}\right)^{2k-1}(\gamma_0 R)\sin[(2k-1)\varphi], \quad 0 < \varphi < \frac{\pi}{2}. \end{aligned} \tag{21}$$

In the plastic region $(\gamma_0 < \gamma_e < \gamma_c)$, the result is

$$\begin{aligned} \psi = &\left\{\frac{1-N}{1+N}\left(\frac{\gamma_0}{\gamma_c}\right)^{1+N}\frac{\gamma_e}{\gamma_0} - \frac{2}{1+N}\left(\frac{\gamma_0}{\gamma_e}\right)^{N}\right\}(\gamma_0 R)\sin\varphi \\ &+ \sum_{k=2}^{\infty}\left\{[\beta_k - (2k-1)]\left(\frac{\gamma_e}{\gamma_0}\right)^{\alpha_k} - [\alpha_k - (2k-1)]\left(\frac{\gamma_e}{\gamma_0}\right)^{\beta_k}\right\}H_k(\gamma_0 R)\sin[(2k-1)\varphi], \\ &0 < \varphi < \frac{\pi}{2}. \end{aligned} \tag{22}$$

In (21) and (22), α_k and β_k are constants given by

$$\alpha_k = \frac{1-N}{2} + \sqrt{\frac{(1-N)^2}{4} + N(2k-1)^2},$$
$$\beta_k = \frac{1-N}{2} - \sqrt{\frac{(1-N)^2}{4} + N(2k-1)^2}. \tag{23}$$

H_k satisfies the following recurrence formula

$$H_2 = -2\left(\frac{\gamma_0}{\gamma_c}\right)^N \Bigg/ \left[(\alpha_2+3)(\beta_2-3)\left(\frac{\gamma_c}{\gamma_0}\right)^{\alpha_2} - (\alpha_2-3)(\beta_2+3)\left(\frac{\gamma_c}{\gamma_0}\right)^{\beta_2}\right],$$
$$H_{k+1} = -\left\{[\alpha_k-(2k-1)][\beta_k-(2k-1)]\left[\left(\frac{\gamma_c}{\gamma_0}\right)^{\alpha_k} - \left(\frac{\gamma_c}{\gamma_0}\right)^{\beta_k}\right]\right\}H_k$$
$$\Bigg/\left\{\left(\frac{\gamma_c}{\gamma_0}\right)^{\alpha_{k+1}}[\alpha_{k+1}+(2k+1)][\beta_k-(2k+1)] - \left(\frac{\gamma_c}{\gamma_0}\right)^{\beta_{k+1}}[\alpha_{k+1}-(2k+1)][\beta_k+(2k+1)]\right\},$$
$$k = 2,3,\ldots \tag{24}$$

and R is

$$R = \frac{1}{2\pi}\left(\frac{K_{III}}{\tau_0}\right)^2. \tag{25}$$

2.3. Stresses in the plastic zone and cohesive zone

The implicit formulas for the stress field in the plastic and cohesive zones can be obtained by substituting (22) into (16). We are most interested in the stress along the crack/cohesive zone plane. In the plastic zone ($x > \rho, y = 0$), $\gamma_x = 0$ and hence $\varphi = 0$. The implicit expression for the stress τ_y is obtained as follows:

$$\frac{x}{R} = \frac{x_0}{R} - \frac{1-N}{1+N}\left(\frac{\tau_0}{\tau_c}\right)^{\frac{1+N}{N}} + \frac{2}{1+N}\left(\frac{\tau_0}{\tau_y}\right)^{\frac{1+N}{N}}$$
$$-\sum_{k=2}^{\infty}\left\{[\beta_k-(2k-1)]\left(\frac{\tau_y}{\tau_0}\right)^{\frac{\alpha_k-1}{N}} - [\alpha_k-(2k-1)]\left(\frac{\tau_y}{\tau_0}\right)^{\frac{\beta_k-1}{N}}\right\}(2k-1)H_k, \tag{26}$$

where x_0 corresponds to zero cohesive traction (physical crack tip). The reason that $x_0 \neq 0$ in the Hodograph transformation is that the physical crack tip may not be located at $x = 0$ as no such conditions are imposed in the transformed boundary conditions (17)–(20). The final solutions of stress and displacement in the strain plane are thus obtained by shifting the physical crack tip to $x = 0$. The x_0 value is determined in the following Eq. (27) so that $x = 0$ corresponds to $\tau_y = 0$.

In the cohesive zone ($0 < x < \rho$), we have $\tau_e = \tau_c$ according to (10) and (14) (note $\chi = \varphi$). The stress is then given by

$$\tau_y = \tau_c \cos\varphi$$

and is related to the coordinate x by

$$\frac{x}{R}=\frac{x_0}{R}+\left(\frac{\tau_0}{\tau_c}\right)^{\frac{1+N}{N}}T_2\left(\frac{\tau_y}{\tau_c}\right)-\frac{1}{2}\sum_{k=2}^{\infty}\left\{\begin{array}{l}[\beta_k-(2k-1)][\alpha_k+(2k-1)]\left(\frac{\tau_c}{\tau_0}\right)^{\frac{\alpha_k-1}{N}}\\ -[\alpha_k-(2k-1)][\beta_k+(2k-1)]\left(\frac{\tau_c}{\tau_0}\right)^{\frac{\beta_k-1}{N}}\end{array}\right\}H_kT_{2k-2}\left(\frac{\tau_y}{\tau_c}\right)$$
$$-\frac{1}{2}\sum_{k=2}^{\infty}\left\{[\alpha_k-(2k-1)][\beta_k-(2k-1)]\left[\left(\frac{\tau_c}{\tau_0}\right)^{\frac{\beta_k-1}{N}}-\left(\frac{\tau_c}{\tau_0}\right)^{\frac{\alpha_k-1}{N}}\right]\right\}H_kT_{2k}\left(\frac{\tau_y}{\tau_c}\right), \tag{27}$$

where $T_k(\cdot)$ are the Chebyshev polynomials of the first kind.

2.4. Cohesive traction–separation relation

In the present study, the cohesive traction in the cohesive zone is assumed to follow (10) and (27) with $\chi=\varphi$. The cohesive traction–separation relation (cohesive law) may be obtained by combining the cohesive traction distribution (27) and the separation displacement δ. According to the Hodograph method, the displacement field is expressed as

$$w=\gamma_e\frac{\partial\psi}{\partial\gamma_e}-\psi. \tag{28}$$

The separation displacement along the cohesive zone may be obtained by substituting (22) into the above equation and letting $\gamma_e=\gamma_c$ as follows:

$$\frac{\delta}{R\gamma_0}=4\left(\frac{\tau_0}{\tau_c}\right)\sqrt{1-\left(\frac{\tau}{\tau_c}\right)^2}$$
$$+2\sum_{k=2}^{\infty}\left\{[\beta_k-(2k-1)](\alpha_k-1)\left(\frac{\tau_c}{\tau_0}\right)^{\frac{\alpha_k}{N}}-[\alpha_k-(2k-1)](\beta_k-1)\left(\frac{\tau_c}{\tau_0}\right)^{\frac{\beta_k}{N}}\right\}H_k$$
$$\times\sin\left[(2k-1)\cos^{-1}\left(\frac{\tau}{\tau_c}\right)\right], \tag{29}$$

where τ is the cohesive traction and can be obtained from (10) and (27). Expression (29) is the cohesive law describing the relationship between the cohesive traction τ and the separation displacement δ.

In the cohesive zone modeling approach, crack extension occurs when the separation at the tail of the cohesive zone (physical crack tip) reaches a critical value at which the cohesive traction usually vanishes. Because the cohesive zone is fully developed, the separation displacement at the physical crack tip is the critical separation and can be obtained by letting $\tau=0$ in (29) as follows:

$$\delta_c=I(N,\frac{\tau_c}{\tau_0})\frac{\tau_0}{\mu}\frac{K_{IIIc}}{2\pi\tau_0^2}, \tag{30}$$

where K_{IIIc} is the critical mode III stress intensity factor and I is given by

$$I=I\left(N,\frac{\tau_0}{\tau_c}\right)$$
$$=4\left(\frac{\tau_0}{\tau_c}\right)+2\sum_{k=2}^{\infty}\left\{[\beta_k-(2k-1)](\alpha_k-1)\left(\frac{\tau_c}{\tau_0}\right)^{\frac{\alpha_k}{N}}-[\alpha_k-(2k-1)](\beta_k-1)\left(\frac{\tau_c}{\tau_0}\right)^{\frac{\beta_k}{N}}\right\}(-1)^{k-1}H_k. \tag{31}$$

For the cohesive zone model (29), the cohesive energy density is

$$\Gamma_c = \int_0^{\delta_c} \tau \, d\delta = \int_0^{\tau_c} \delta \, d\tau = \pi \tau_0 R \gamma_0 = \frac{K_{IIIc}^2}{2\mu}, \tag{32}$$

i.e., the cohesive energy density is the critical energy release rate.

The size of the fully developed cohesive zone may be determined from (27) by subtracting the x-value corresponding to $\tau_y = 0$ from that corresponding to $\tau_y = \tau_c$ with the result

$$\begin{aligned}\frac{\rho}{R} = {} & 2\left(\frac{\tau_0}{\tau_c}\right)^{\frac{1+N}{N}} - \sum_{k=2}^{\infty}\left\{[\beta_k - (2k-1)]\left(\frac{\tau_c}{\tau_0}\right)^{\frac{\alpha_k - 1}{N}} - [\alpha_k - (2k-1)]\left(\frac{\tau_c}{\tau_0}\right)^{\frac{\beta_k - 1}{N}}\right\}(2k-1)H_k \\ & + \sum_{k=2}^{\infty}\left\{[\beta_k - (2k-1)]\alpha_k\left(\frac{\tau_c}{\tau_0}\right)^{\frac{\alpha_k - 1}{N}} - [\alpha_k - (2k-1)]\beta_k\left(\frac{\tau_c}{\tau_0}\right)^{\frac{\beta_k - 1}{N}}\right\}(-1)^{k-1}H_k.\end{aligned} \tag{33}$$

2.5. Stress field in the elastic zone and plastic zone contour

The stress field in the elastic zone can be obtained by substituting (21) into (16)

$$\begin{aligned}\frac{x}{R} &= \frac{x_0}{R} + \frac{1-N}{1+N}\left[1 - \left(\frac{\tau_0}{\tau_c}\right)^{\frac{1+N}{N}}\right] + \left(\frac{\tau_0}{\tau_e}\right)^2 \cos(2\varphi) - \sum_{k=2}^{\infty}(\beta_k - \alpha_k)(2k-1)H_k\left(\frac{\tau_e}{\tau_0}\right)^{2k-2}\cos[(2k-2)\varphi], \\ \frac{y}{R} &= \left(\frac{\tau_0}{\tau_e}\right)^2 \sin(2\varphi) + \sum_{k=2}^{\infty}(\beta_k - \alpha_k)(2k-1)H_k\left(\frac{\tau_e}{\tau_0}\right)^{2k-2}\sin[(2k-2)\varphi].\end{aligned} \tag{34}$$

By neglecting the higher order terms of τ_e/τ_0 and keeping only the first term in (34), we can obtain the stress field at distances far away from the crack tip as follows

$$\tau_e = \frac{K_{III}}{\sqrt{2\pi r_1}}, \quad \varphi = \frac{\theta_1}{2}, \tag{35}$$

where (r_1, θ_1) are the polar coordinates defined by

$$\begin{aligned}x - x_0 - \frac{1-N}{1+N}\left(1 - \left(\frac{\tau_0}{\tau_c}\right)^{\frac{1+N}{N}}\right)\frac{K_{III}^2}{2\pi\tau_0^2} &= r_1\cos\theta_1, \\ y &= r_1 \sin\theta_1\end{aligned} \tag{36}$$

(35) and (36) together with (14) indicate that the elastic stress field far away from the crack tip is the usual square root singular field in LEFM with the crack tip shifted to $(x, y) = ((1-N)/(1+N)\left(1 - (\tau_0/\tau_c)^{(1+N)/N}\right)K_{III}^2/(2\pi\tau_0^2) + x_0, 0)$.

The plastic zone contour, or the elastic–plastic boundary, can be obtained from (34) by setting $\tau_e = \tau_0$

$$\begin{aligned}\frac{x}{R} &= \frac{x_0}{R} + \frac{1-N}{1+N}\left[1 - \left(\frac{\tau_0}{\tau_c}\right)^{\frac{1+N}{N}}\right] + \cos(2\varphi) - \sum_{k=2}^{\infty}(2k-1)(\beta_k - \alpha_k)H_k\cos[(2k-2)\varphi], \\ \frac{y}{R} &= \sin(2\varphi) + \sum_{k=2}^{\infty}(2k-1)(\beta_k - \alpha_k)H_k\sin[(2k-2)\varphi], \quad 0 \leqslant \varphi \leqslant \frac{\pi}{2}.\end{aligned} \tag{37}$$

2.6. Numerical results and discussion

Fig. 2 shows the distribution of the normalized shear stress τ_y/τ_0 along the crack extended line including the cohesive zone for $N = 0.3$. The peak values of cohesive traction τ_c are taken as 1.5, 2.0 and 2.5 times the yield stress τ_0 in Fig. 2a, b and c, respectively. The corresponding stress fields in EPFM (Rice, 1968, no

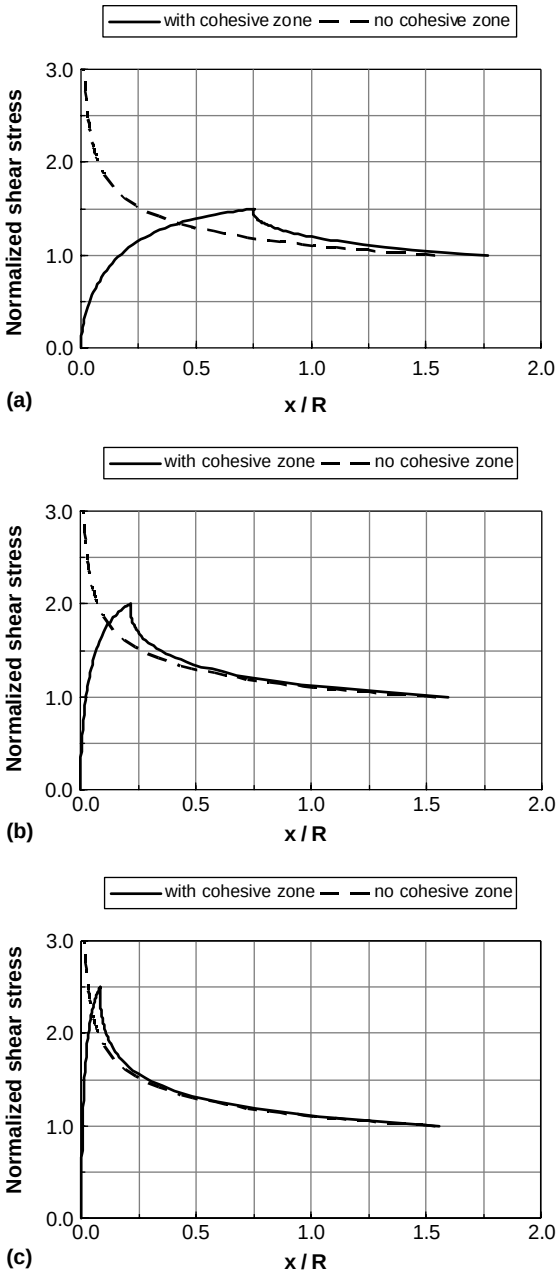

Fig. 2. Stress distribution along the crack extended line for $N = 0.3$: (a) $\tau_c/\tau_0 = 1.5$, (b) $\tau_c/\tau_0 = 2.0$, (c) $\tau_c/\tau_0 = 2.5$.

cohesive zone) are also shown. It can be seen from the figure that when the cohesive zone is considered, the shear stress increases from τ_0 at the elastic–plastic boundary to τ_c at the cohesive zone tip, and then gradually decreases to zero at the physical crack tip (the tail of the cohesive zone). For the traction ratio of $\tau_c/\tau_0 = 2.5$, the stress matches with the singular solution in EPFM in most part of the plastic zone as indicated in Fig. 2c (the cohesive zone is relatively small compared with the plastic zone in this case, see Fig. 5). For the lower traction ratios of τ_c/τ_0, however, the stress distribution is significantly altered by the consideration of the cohesive zone as shown in Fig. 2a and b.

For small scale yielding, the stress distribution in the plastic zone is not critical in predicting fracture. For medium or large scale yielding, however, the stress distribution may play a significant role. For the cohesive zone approach and EPFM to produce identical predictions on fracture, the stress distribution in most part of the plastic zone with a cohesive zone should match that in EPFM. The implications of the results in Fig. 2 are that the peak cohesive traction should be greater than about 2.5 times yield stress to fulfill the requirement of the stress distribution match.

Fig. 3 again shows the distribution of the normalized shear stress τ_y/τ_0 along the crack extended line. The hardening exponent is now $N = 0.1$. For this weak hardening material case, the stress matches with the singular solution in EPFM in most part of the plastic zone, and hence, only the stress for $\tau_c = 1.5\tau_0$ is shown. The results in Figs. 2 and 3 show that the stress basically agree with that in EPFM at distances (away from the crack tip) greater than two times cohesive zone size.

Fig. 4a shows the plastic zone contour (elastic/plastic boundary) for $N = 0.3$ and $\tau_c/\tau_0 = 1.5$. The case for $\tau_c/\tau_0 = 2.5$ is shown in Fig. 4b. It is observed that both the plastic zone size and the shape are not significantly different from the circular zone found in EPFM, especially when the traction ratio τ_c/τ_0 is high. The plastic zone extends ahead of the crack tip a bit more in the presence of the cohesive zone.

Fig. 5 shows the ratio of cohesive zone length to the plastic zone size ahead of the crack tip versus the traction ratio τ_c/τ_0. The cohesive zone is relatively small compared with the plastic zone in the weak strain hardening case ($N = 0.1$). For the modestly hardening case ($N = 0.3$), however, the cohesive zone becomes a significant portion of the plastic zone, especially when the traction ratio τ_c/τ_0 is low. For example, the cohesive zone length is about 43% of the plastic zone size ahead of the crack in the case of $\tau_c/\tau_0 = 1.5$.

Fig. 6 shows the cohesive traction–separation curve calculated from (29). The cohesive model follows a softening path with the maximum traction at the start of separation. Compared with the linear softening model, the cohesive traction in the present specific model decreases slowly at the initial stage of separation.

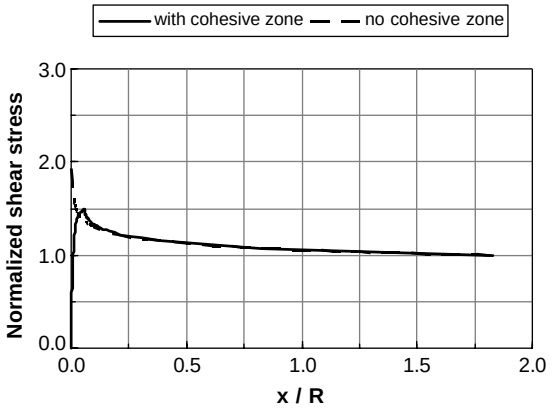

Fig. 3. Cohesive stress distribution along the crack extended line for $N = 0.1$ ($\tau_c/\tau_0 = 1.5$).

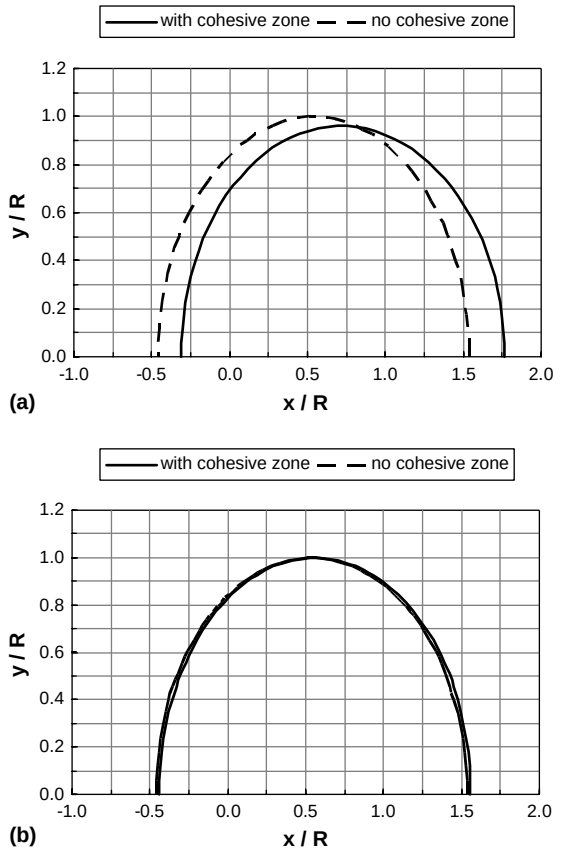

Fig. 4. Plastic zone contour for $N = 0.3$: (a) $\tau_c/\tau_0 = 1.5$, (b) $\tau_c/\tau_0 = 2.5$.

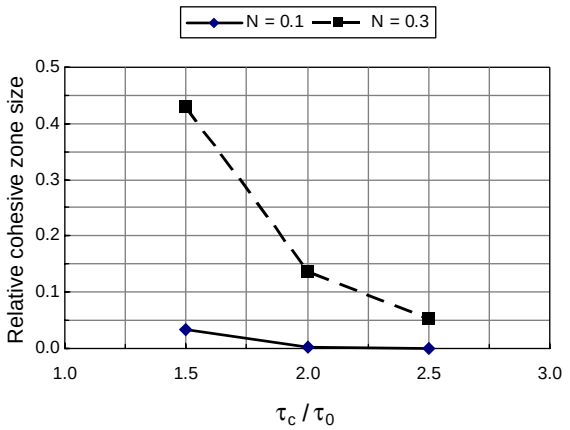

Fig. 5. Ratio of the cohesive zone length to the plastic zone size ahead of the crack tip.

The drop in the cohesive traction accelerates towards the maximum separation at which the traction vanishes.

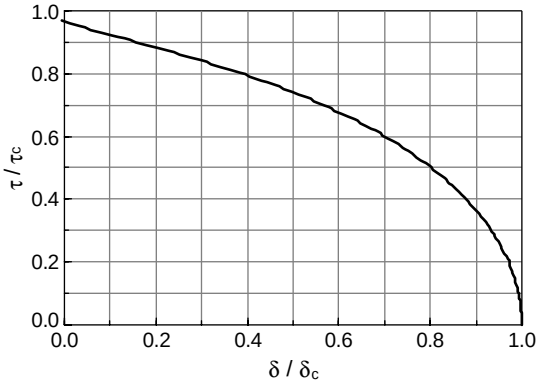

Fig. 6. Normalized cohesive traction–separation curve ($N = 0.3$, $\tau_c/\tau_0 = 2.5$).

3. Cohesive zone modeling and LEFM

For fracture of brittle materials described by LEFM, the cohesive zone modeling approach becomes equivalent to LEFM if the K-dominance zone still exists around the crack tip and the cohesive energy density becomes the critical energy release rate (Rice, 1968; Wang and Sun, 2004). In this section we examine qualitatively the restriction on the peak cohesive traction when the cohesive zone approach and LEFM are approximately equivalent.

When the background material is elastic, a simple closed form solution of the crack/cohesive zone problem can be obtained from the series solution given in Section 2 by letting $N = 1$ and $\tau_0 = \tau_c$. The constants α_k, β_k and H_k now become

$$\begin{aligned} &\alpha_k = 2k - 1, \\ &\beta_k = -(2k-1), \quad k \geqslant 1, \end{aligned} \tag{38}$$

$$\begin{aligned} &H_2 = 1/18, \\ &H_k = 0, \quad k \geqslant 3. \end{aligned} \tag{39}$$

Substituting the above constants into (21), we have the expression for the strain function

$$\psi = -\frac{\gamma_0}{\gamma_e}(\gamma_0 R)\sin\varphi - \frac{1}{3}\left(\frac{\gamma_e}{\gamma_0}\right)^3(\gamma_0 R)\sin(3\varphi), \quad 0 < \varphi < \frac{\pi}{2}. \tag{40}$$

The effective stress τ_e and the phase angle φ are related to the coordinates (x, y) by

$$\begin{aligned} \frac{x}{R} &= \frac{x_0}{R} + \left[\left(\frac{\tau_0}{\tau_e}\right)^2 + \left(\frac{\tau_e}{\tau_0}\right)^2\right]\cos(2\varphi), \\ \frac{y}{R} &= \left[\left(\frac{\tau_0}{\tau_e}\right)^2 - \left(\frac{\tau_e}{\tau_0}\right)^2\right]\sin(2\varphi). \end{aligned} \tag{41}$$

The traction τ_y in the cohesive zone follows (41) by taking $\tau_e = \tau_0$

$$\frac{x}{R} = \frac{x_0}{R} + 2\cos\left[2\cos^{-1}\left(\frac{\tau_y}{\tau_c}\right)\right] \tag{42}$$

and the separation displacement of the cohesive surfaces is related to the cohesive traction by

$$\frac{\delta}{R\gamma_0} = 4\sqrt{1-\left(\frac{\tau}{\tau_c}\right)^2} - \frac{4}{3}\sin\left[3\cos^{-1}\left(\frac{\tau}{\tau_c}\right)\right]. \tag{43}$$

The size of the fully developed cohesive zone is obtained as the difference between the x-values in (42) corresponding to $\tau_y = \tau_0$ and $\tau_y = 0$

$$\rho = \frac{4}{\pi}\frac{\mu\Gamma_c}{\tau_c^2}, \tag{44}$$

where $\Gamma_c = K_{IIIc}^2/(2\mu)$ is the cohesive energy density which is set to equal the energy release rate in LEFM.

The above discussion is for the mode III problem. For mode I crack problems with a softening cohesive zone, Hillerborg et al. (1976) proposed a characteristic length of the cohesive zone

$$l_{coh} = \frac{E\Gamma_c}{(1-\nu^2)\sigma_c^2}, \tag{45}$$

where Γ_c is the cohesive energy density, σ_c is the peak cohesive traction, E is Young's modulus and ν is Poisson's ratio. It is clear that the length parameter of (45) is consistent with (44) from the present analytical solution in terms of the order of magnitude.

The equivalency between the cohesive zone approach and LEFM requires that there exists a K-dominance zone around the crack tip and the cohesive energy density is the critical energy release rate. Considering that the cohesive zone may influence the stress distribution at locations (away from the crack tip) two times the cohesive zone size, the above equivalent conditions may be approximately expressed as

$$l_{coh} = \frac{K_{Ic}^2}{\sigma_c^2} < \frac{R_k}{2}, \tag{46}$$

where R_k is the K-dominance zone size and $K_{Ic} = \sqrt{EG_{Ic}/(1-\nu^2)}$ with the critical energy release rate $G_{Ic} = \Gamma_c$. Since R_k is generally at least one order of magnitude smaller than the crack length a_0, the inequality (46) may be roughly expressed as

$$l_{coh} = \frac{K_{Ic}^2}{\sigma_c^2} < \frac{a_0}{20}. \tag{47}$$

Since a_0 is a structural parameter, the condition (47) is a structural property rather than a material characteristic. That is, σ_c is a structural parameter. For example, for a fine grained ceramic material with an average grain size of 1 μm, a crack of length a_0 roughly 50 times the grain size may be treated by LEFM. For a $K_{Ic} = 2$ MPa m$^{1/2}$, condition (47) thus requires that the peak cohesive traction satisfy

$$\sigma_c > \frac{K_{Ic}}{\sqrt{a_0/10}} \approx 1265 \text{ MPa}.$$

For the same material with a macroscopic crack of $a_0 = 1$ mm, the restriction to the peak cohesive traction now becomes $\sigma_c > 283$ MPa. In summary, smaller cracks require a higher peak cohesive traction than that for longer cracks if similar fracture initiation loads are predicted by the two approaches.

4. Concluding remarks

A mode III crack with a fully developed cohesive zone in an elastic power-law hardening material is first studied under the small scale yielding condition. The stress and strain fields in the plastic zone and the

cohesive traction and separation displacement in the cohesive zone are obtained using a special cohesive law that follows a softening path with the peak traction at the start of separation process. It is found that for a modestly hardening material with a hardening exponent of $N = 0.3$, the stress distributions with and without the cohesive zone are significantly different in a large portion of the plastic zone if the peak cohesive traction is less than two times yield stress. The implications of these results to medium and large scale yielding are that the peak cohesive traction should be greater than about 2.5 times yield stress to fulfill the requirement of the stress distribution match so that the cohesive zone approach and the classical approach of EPFM produce similar predictions on fracture.

References

Barenblatt, G.I., 1962. The mathematical theory of equilibrium cracks in brittle fracture. Advances in Applied Mechanics 7, 55–129.

de Borst, R., 2003. Numerical aspects of cohesive zone models. Engineering Fracture Mechanics 70, 1743–1757.

Dugdale, D.S., 1960. Yielding of steel sheets containing slits. Journal of the Mechanics and Physics of Solids 8, 100–104.

Elices, M., Guinea, G.V., Gomez, J., Planas, J., 2002. The cohesive zone model: advantages, limitations and challenges. Engineering Fracture Mechanics 69, 137–163.

Hillerborg, A., Modeer, M., Petersson, P.E., 1976. Analysis of crack formation and crack growth in concrete by means of fracture mechanics and finite elements. Cement and Concrete Research 6, 773–782.

Jin, Z.-H., Sun, C.T., 2005a. Cohesive zone modeling of interface fracture in elastic bi-materials. Engineering Fracture Mechanics 72, 1805–1817.

Jin, Z.-H., Sun, C.T., 2005b. Cohesive fracture model based on necking. International Journal of Fracture, in press.

Needleman, A., 1987. A continuum model for void nucleation by inclusion debonding. ASME Journal of Applied Mechanics 54, 525–531.

Ortiz, M., Pandolfi, A., 1999. Finite-deformation irreversible cohesive elements for three-dimensional crack-propagation analysis. International Journal for Numerical Methods in Engineering 44, 1267–1282.

Rice, J.R., 1968. Mathematical analysis in the mechanics of fracture. In: Liebowitz, H. (Ed.), Fracture, vol. 2. Academic Press, New York, pp. 191–311.

Roy, Y.A., Dodds Jr., R.H., 2001. Simulation of ductile crack growth in thin aluminum panels using 3-D surface cohesive elements. International Journal of Fracture 110, 21–45.

Scheider, I., Brocks, W., 2003. The effect of the traction separation law on the results of cohesive zone crack propagation analyses. Key Engineering Materials 251-2, 313–318.

Tvergaard, V., Hutchinson, J.W., 1992. The relation between crack growth resistance and fracture process parameters in elastic–plastic solids. Journal of the Mechanics and Physics of Solids 40, 1377–1392.

Wang, C.Y., Sun, C.T., 2004. Energy variation during crack growth in cohesive fracture model. In: Proceedings of the 4th European Congress on Computational Methods in Applied Sciences and Engineering (ECCOMAS 2004), Jyvaskyla, Finland.

Xu, X.P., Needleman, A., 1994. Numerical simulations of fast crack growth in brittle solids. Journal of the Mechanics and Physics of Solids 42, 1397–1434.